ACCSCIENCE PUBLISHING

International Journal of Bioprinting

RESEARCH ARTICLE

Alginate–gelatin–silk fibroin-containing patches improve cardiac function in an *in vivo* myocardial infarction murine model

Laura Vettori[1,2], Ashton Matthee[1,2], Clara Liu Chung Ming[1,2], Niina Matthews[1,2], Dominik Beck[1], Timothy Couttas[3], Hien Ahn Tran[4], Jelena Rnjak-Kovacina[4], and Carmine Gentile[1,2]*

[1]School of Electrical, Mechanical and Biomedical Engineering, Faculty of Engineering and Information Technology, University of Technology Sydney, Sydney, New South Wales, Australia

[2]Cardiovascular Regeneration Group, The Heart Research Institute, Sydney, New South Wales, Australia

[3]Brain and Mind Centre, The University of Sydney, Sydney, New South Wales, Australia

[4]Graduate School of Biomedical Engineering, Faculty of Engineering, University of New South Wales, Sydney, New South Wales, Australia

Abstract

Transplantation of patches based on alginate and gelatin biomaterials represents a promising approach for improving cardiac function *in vivo*. To enhance the long-term durability and mechanical properties of alginate–gelatin patches, silk fibroin was added to the formulation, and 3D-printed alginate–gelatin–silk fibroin patches without cells were transplanted into an *in vivo* myocardial infarction murine model. The focus of this study is to evaluate whether the addition of silk fibroin to alginate–gelatin hydrogels can protect against the reduction in cardiac function after myocardial infarction. Mice were divided into four experimental groups: sham, myocardial infarction, myocardial infarction with the transplanted alginate–gelatin patch, and myocardial infarction with the transplanted alginate–gelatin–silk fibroin patches. The ultrasound analyses demonstrated that silk fibroin-containing patches increased the left ventricular ejection fraction percentage by 20% in infarcted mice. Furthermore, histological and transcriptomic analyses demonstrated that alginate–gelatin–silk fibroin patches stimulated tissue-repairing processes, reduced cardiac fibrosis, promoted cardiac remodeling, increased inflammation-regulating gene expression, and recapitulated cardiac function and tissue homeostasis in myocardial infarction mice. Altogether, our *in vivo* findings support the biofabrication of advanced cardiac tissues containing alginate–gelatin–silk fibroin for tissue engineering and regenerative medicine, representing a potential therapeutic approach for patients with myocardial infarction.

Keywords: Silk fibroin; Hydrogels; Biofabrication; Myocardial infarction

***Corresponding author:**
Carmine Gentile
(Carmine.Gentile@uts.edu.au)

Citation: Vettori L, Matthee A, Liu Chung Ming C, *et al*. Alginate–gelatin–silk fibroin-containing patches improve cardiac function in an *in vivo* myocardial infarction murine model. *Int J Bioprint*. 2026;12(5):026250260. doi: 10.36922/IJB026250260

Received: June 19, 2026

Revised: July 16, 2026

Accepted: July 20, 2026

Published online: July 20, 2026

Copyright: © 2026 Author(s). This is an Open-Access article distributed under the terms of the Creative Commons Attribution License, permitting distribution, and reproduction in any medium, provided the original work is properly cited.

Publisher's Note: AccScience Publishing remains neutral with regard to jurisdictional claims in published maps and institutional affiliations.

1. Introduction

Cardiovascular disease remains the leading cause of global morbidity and mortality.[1] Myocardial infarction (MI) is one of the most prevalent cardiovascular diseases and leads to several pathophysiological changes to the heart, such as inflammation,

fibrosis, and tissue remodeling.[2] Following an MI, the limited regenerative ability of the adult heart leads to the permanent loss of cardiomyocytes and impairment of cardiac function, resulting in heart failure.[3,4]

Macrophages play an important role in cardiac remodeling following injury, activating cardiac fibroblasts, which deposit extracellular matrix (ECM) components to form a collagenous tissue scar.[5-8] This process of attempted cardiac tissue repair is known as myocardial fibrosis.[3,9] The scar reduces tissue elasticity and reduces the heart's contractile ability.[5-7,10,11]

Three-dimensional (3D) bioprinting has emerged as a promising solution to facilitate the replacement of fibrotic tissue in heart failure patients, *via* the bioengineering of personalized cardiac tissues for patients who have had MI.[3,12,13] Among other tissues and organs, 3D-printed tissues have shown promise for potential applications in humans.[14-16] In the heart, this cutting-edge technique involves the implantation of a 3D cardiac tissue patch onto the damaged area, aiming to enhance the regenerative capacity of the injured heart and restore function.[17] Moreover, cardiac patches can reverse the progression of pathology after MI, reducing the scar tissue area, promoting angiogenesis, reinforcing the mechanical properties of the tissue, and preventing patients from developing heart failure.[2,18] The convergence of advanced biomaterials and emerging bioprinting technologies has led to a new era of regenerative medicine, potentially revolutionizing the treatment of MI and offering new avenues for cardiac repair and regeneration. For example, alginate (Alg)–gelatin (Gel) (AlgGel) hydrogels have already been explored for cardiac tissue bioprinting, with high biocompatibility to embedded induced pluripotent stem cell-derived cardiac spheroids and approximating the complex cardiac microenvironment *in vitro*.[12,13,17] In particular, previous studies in our team have demonstrated that printed AlgGel patches have shown promise in protecting against the reduction in cardiac function in MI mice.[12,13,17] However, AlgGel patches have sub-optimal mechanical properties and tend to degrade in a physiological environment. This may limit their use for *in vivo* applications.[9]

Silk fibroin (SF) is a strong and stable polymer that has been extensively explored for vascular applications, both *in vitro* and *in vivo*. Produced by the *Bombyx mori* silkworm, SF has emerged as a promising biomaterial for cardiac tissue engineering applications, owing to its exceptional cytocompatibility, biodegradability, and mechanical properties.[4,9,19] In addition, given its tunable properties and low immunogenicity in the human body, it has shown potential to provide an effective treatment for MI. Nevertheless, SF solutions require modifications to be effective as standalone printing components. AlgGel hydrogels have mechanically soft properties;[9,13,20] therefore, SF has been incorporated into AlgGel hydrogels to improve their mechanical properties and printability and modulate cardiac muscle contractile function. In fact, our laboratory's *in vitro* results demonstrated that adding 1% (w/v) SF to 4% Alg–8% Gel hydrogels enhanced their elastic properties and exhibited improved contractile activity of cardiac spheroids embedded in AlgGel hydrogels.[9] Thus, following our previous studies using AlgGel *in vivo*[17] and now in combination with SF,[9] this study focuses on the use of 1% SF added to 4% Alg–8% Gel hydrogels.

This study hypothesizes that the addition of 1% SF to AlgGel patches (AlgGelSF) improves cardiac function *in vivo*. In particular, we evaluated the effect of AlgGelSF patches on cardiac function to identify whether the enhanced mechanical properties can improve cardiac function after MI (Figure 1). Additionally, we investigated the complex interaction between 3D-printed AlgGelSF patches and myocardial tissue post-MI, and its effects on cardiac fibrosis, cell survival, and gene expression involved in cardiac tissue remodeling.

Here, we showed the effects of AlgGelSF patches implanted on the apex of the MI mice hearts (Figure 1) following a permanent left anterior descending (LAD) artery ligation surgical procedure on *RAG1* immunodeficient mice. This model, devoid of functional T- and B-lymphocytes, offers a controlled environment for studying the interaction between the implanted constructs and the host tissue without the confounding variables of an intact immune response.[21]

Investigating the *in vivo* post-MI response to 3D-printed AlgGelSF patches in *RAG1* immunodeficient mice not only enhances our understanding of the regenerative potential of these constructs but also provides crucial insights into their future clinical translation. Overall, this research endeavors to develop advanced therapeutic strategies for MI patients by combining biomaterial science, bioprinting technology, and immunodeficient murine models.

2. Materials and methods

2.1. Materials

Bombyx mori silkworm cocoons were purchased from Sato Yama (Japan), while sodium alginate and Gel from bovine skin were purchased from Sigma-Aldrich (United States of America [USA]). Ketamine, xylazine, and atropine solutions for *in vivo* studies were purchased from Troy Laboratories (Australia).

2.2. Silk fibroin isolation and silk fibroin-containing hybrid hydrogel preparation and crosslinking

Silk fibroin protein was extracted as previously described

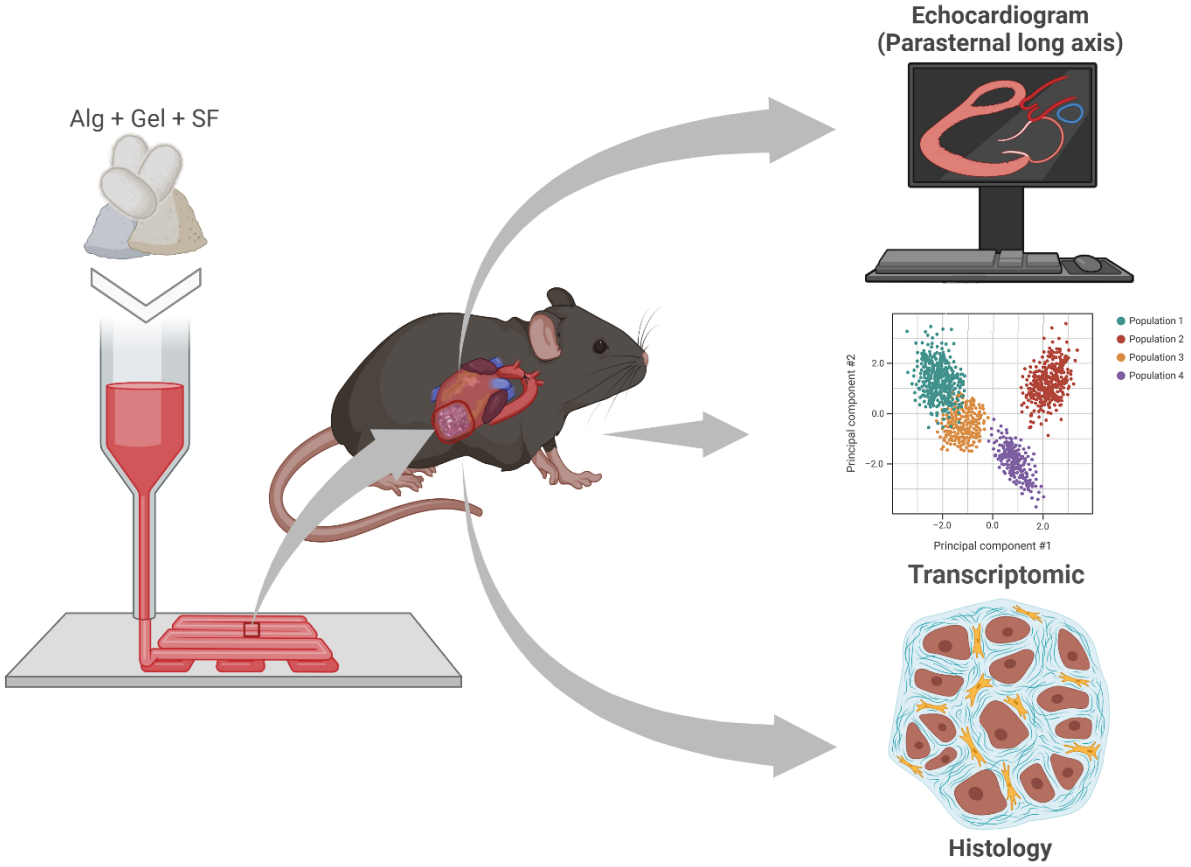


Figure 1. Schematic representation of the fabrication of AlgGelSF patches and the evaluation of their effects on cardiac function. AlgGelSF hydrogels were used to print cardiac patches, which were implanted into a mouse MI model. Echocardiography was used to evaluate the effect of the patch on ejection fraction, while heart tissue sections were used to evaluate fibrotic and molecular changes via histological and transcriptomic analyses.
Abbreviations: Alg: Alginate; Gel: Gelatin; MI: Myocardial infarction; SF: Silk fibroin.

to obtain an aqueous protein solution.[22,23] *B. mori* silkworm cocoons were degummed in 2 L of 0.02 M sodium carbonate (Na_2CO_3; Sigma-Aldrich) solution at high temperature (90 °C–100 °C). Following rinsing and drying, degummed fibers were dissolved in 9.3 M lithium bromide (LiBr; Sigma-Aldrich) solution at 60 °C (4 mL per 1 g of fibers). The last step involved a dialysis process using a cellulose membrane (1 cm/3 mL SF solution) (SnakeSkinTM Dialysis Tubing; Thermo Fisher Scientific, USA), and a three-cycle centrifugation (8,700 rpm, 4 °C, 15 min each step). The SF aqueous solution obtained was 7%–9% (w/v).[9] Four grams of sodium alginate (Sigma-Aldrich) and 8 g of Gel from bovine skin powders (Sigma-Aldrich) were dissolved in 100 mL of Dulbecco's modified Eagle's medium (DMEM)–high glucose solution (Sigma-Aldrich), containing 1% (v/v) penicillin–streptomycin (Sigma-Aldrich) and 1% (v/v) *L*-glutamine (Sigma-Aldrich), at 60 °C under gentle rotation.[9] Based on the previous *in vitro* results,[9] 1% (w/v) SF concentration was then mixed with 4% (w/v) Alg–8% (w/v) Gel (AlgGel) hydrogels, and the final 4% Alg–8% Gel–1% SF (AlgGelSF) formulation was crosslinked using a 2% (w/v) calcium chloride ($CaCl_2$; Sigma-Aldrich) in Dulbecco's phosphate-buffered saline (DPBS; Sigma-Aldrich).[9,13]

2.3. 3D-printed AlgGelSF-containing hybrid hydrogels and patches preparation for *in vivo* transplantation and tensile strength testing

AlgGelSF-containing inks were printed ($n \geq 6$) using the BIO X6 extrusion-based bioprinter (CELLINK, Sweden). The 3D printing process protocol was optimized based on previous studies.[9,17] BIO X6 cartridges (CELLINK) were autoclaved, then placed under a biosafety cabinet with 22-gauge polypropylene nozzles and sterilized using the built-in UV light cycle. AlgGel and AlgGelSF solutions were warmed at 37 °C before 3 mL of hydrogel was loaded into the bioprinter cartridge. Each AlgGelSF hydrogel concentration was extruded through a 22-gauge

nozzle into 6-well plates. Samples were 3D printed with a rectilinear pattern as a lattice of 20 mm × 20 mm × 0.82 mm (width × length × height) with two layers of 0.41 mm, established by a G-code created using the GPad code editor integrated in DNA Studio 4 software (CELLINK), with an infill grid density of 25% (Video S1). The printing parameters used were: pneumatic tool head set to 30 °C, print bed temperature set to 10 °C, and extrusion speed set to 9 mm/s. Pressure was adjusted during printing and ranged from 10 to 20 kPa. Following gelation and a one-hour crosslinking process, DMEM was added to each well, and patches were incubated at 37 °C with 5% (v/v) CO_2.[9] To prevent patch disintegration, the plate's movement was minimized. DMEM was carefully replaced with fresh medium at low volume every 2–3 days, and the patches were cultured until the day of *in vivo* transplantation (up to 5 days). The 3D-printed patches were cut into 4 mm × 4 mm pieces using a sterile surgical scalpel blade size 11 (Sigma-Aldrich) immediately before surgery. Each piece was placed on sterile aluminum foil and transferred to the procedure bench before transplantation.

Some additional patches were 3D printed for tensile-strength testing, and the printing protocol was optimized following the steps described above. Samples were 3D printed into Petri dishes using a linear infill pattern with two layers of 0.41 mm and an infill density of 20%. AlgGel patches were printed with a size of 60 mm × 50 mm × 0.82 mm (width × length × height), while AlgGelSF patches were printed with a size of 60 mm × 20 mm × 0.82 mm. The pneumatic tool head was set at 28 °C with a temperature controller. The print bed temperature was set to 10 °C, the extrusion speed to 5 mm/s, and the pressure was adjusted during the process between 35 and 45 kPa. Following crosslinking, AlgGel and AlgGelSF patches were used for strength testing (fatigue testing) using an ATMS Dynamic Culture Technology System (Taihoya, Taiwan) (Figure S1E–F). Patches were carefully transferred to the Taihoya membranes using spatulas; membranes with AlgGelSF patches were fixed to the instrument and submerged in DMEM or DPBS. The instrument was set at 12 V, 1 Hz, 60 bpm, and 20% dynamic stretch to mimic the conditions of a healthy human heart (Videos S2 & S3). Patches were monitored for up to 24 hours.

2.4. Murine model of myocardial infarction and 3D-printed patch transplantation

All procedures were approved by the Animal Ethics Committee at the University of Technology Sydney (ETH19-4338). The surgical procedures were performed according to our well-established protocol[17,24] on B6.RAG-1 immunodeficient (B, T cell-depleted) male mice (Australian BioResources, Australia), aged 9–10 weeks. A total of 28 mice were used in this study. Mice were randomly divided into four experimental groups: (a) Sham, (b) MI, (c) MI + AlgGel patch, and (d) MI + AlgGelSF patch.

The anesthetic solution comprised ketamine (40 mg/kg), xylazine (5 mg/kg), and atropine (0.15 mg/kg), with 100 µL injected via intraperitoneal injection. Once the mouse was fully anesthetized (after about 10 min), it was placed in a chamber inhaling 3 L/min isoflurane and 2 L/min oxygen. Following intubation, the mouse was carefully placed on a heated surface and connected to a PhysioSuite ventilator (Kent Scientific Corporation, USA) to maintain constant anesthesia (isoflurane: 0–2 L/min; oxygen: 1–2 L/min) throughout the procedure. A few drops of betadine were applied to the mouse's chest, and 100 µL of buprenorphine (0.08 mg/kg; Temvet, Troy Laboratories Pty Ltd, Australia) in 0.1 mL of 0.9% saline solution was administered via subcutaneous injection. All surgical procedures were performed using a microscope to aid in visualization (Leica 651, Germany). Initially, a left thoracotomy was performed to access the mouse's heart. During the sham procedure, a silk suture 7-0 (PERMA-HAND SILK, Ethicon, USA) was passed under the LAD artery, and it was tied loosely without occluding the artery, while MI was performed *via* permanent LAD ligation (occlusion of the LAD artery). Following the MI surgery, AlgGel and AlgGelSF patches were immediately transplanted onto the infarcted tissue (Video S4). Then, the muscles and skin layers of the chest were closed with a Prolene suture 6-0 (ETHICON). Once the surgery was finished, isoflurane was stopped, and the wound was wiped with betadine and ethanol. Then, 100 µL of Antisedan (atipamezole, 1 mg/kg), 100 µL of Lasix (furosemide, 8 mg/kg), and 500 µL of sodium chloride solution (0.9% saline) were injected subcutaneously at different sites on the mouse. Bupivacaine (2 mg/mL in 0.9% saline solution) was also applied to the wound, and the mouse's eyes were lubricated with Poly-Tears Lubricating eye drops (Alcon, USA). Once the mouse began breathing independently, it was transferred to a chamber with 2 L/min of oxygen and monitored until fully recovered, then transferred to a cage with water and jelly food.

During the postoperative period (the first week immediately after the procedure), mice were injected twice daily for the first three days and once daily the following four days with buprenorphine (0.08 mg/kg) via subcutaneous injection by a trained researcher (L. V.).

2.5. Mice echocardiography (heart ultrasound).

Echocardiography (ultrasound [US]) was performed with a Vevo 3100 Preclinical Imaging System (FUJIFILM

VisualSonics, Canada).[25] Mice were imaged at day 0 (baseline), day 14 (midpoint), and day 28 (endpoint).[17]

Before each US imaging, mice were weighed and then anesthetized (isoflurane: 3 L/min, oxygen: 2 L/min). Once anesthetized, mice were transferred to the pre-warmed (37 °C) Fujifilm VisualSonics platform, where each mouse was placed supine and kept anesthetized through a nose cone with 2 L/min isoflurane and 2 L/min oxygen. A small amount of Conductive Gel (Livingstone, Australia) was applied to the feet of each mouse before it was taped to the four electrodes on the platform. Once the mouse was immobilized, shaving cream (Hair Removal Cream, Nair, USA) was applied to its chest. After a few minutes, the cream was removed with gauze swabs (Livingstone), and some US gel (Aquasonic Ultrasound Transmission Gel, Parker, USA) was applied to the mouse's shaved chest. During the parasternal long-axis view, the transducer was rotated to an 11 o'clock position, and B-mode cardiac cycles were acquired. Throughout the echocardiography, the mouse's heart was maintained at >400 bpm (beats per minute), while cardiac cycles were recorded.[17,26]

Ultrasound data related to the parasternal long-axis view were analyzed to measure the left ventricular ejection fraction (LVEF) using VevoLAB 5.7.1 software (FUJIFILM VisualSonics) by outlining the diastolic and systolic cycles ($n \geq 4$/group) of the left ventricle using either the manual or the automatic (AutoLV) mode. A VisualSonics data specialist from Fujifilm validated the data.

2.6. Sample collection for histological, hypertrophy, and transcriptomic analyses of the mouse hearts

At day 28 (endpoint), mice were euthanized, and tissue samples were collected to perform histological and transcriptomic analyses.[17] Mice were weighed, then placed under anesthesia (isoflurane: 5 L/min, oxygen: 2 L/min) using a cone. The chest was opened and the heart exposed. Blood was aspirated with a 21-gauge needle and collected into tubes containing heparin. The heart was then collected and weighed. Transverse slices (1 mm thick) of the left ventricle were obtained with a sharp blade. Heart slices were added to Eppendorf tubes with a 10% neutral buffer of formalin and kept at room temperature for histological analyses, or added to Eppendorf tubes and kept at −80 °C in liquid nitrogen until RNA isolation for transcriptomic analyses.

Finally, the tibia was isolated, and its length was measured using a 155 mm digital caliper (Aus Electronics Direct, Australia) for hypertrophy analyses. Hypertrophy was evaluated by plotting the ratios of heart weight to body weight and heart weight to tibia length ($n \geq 4$/group). Heart weights were normalized to body weights and tibia lengths to assess hypertrophic tissue increase in mice post-MI.

2.7. Histological analyses

2.7.1. Sample preparation and tissue processing

Heart tissue slices for histological staining were stored in 10% neutral buffered formalin for 10 days, then washed three times with 0.01% (v/v) sodium azide in phosphate-buffered saline (PBSA). At the same time, histology cassettes were prepared and labeled with each mouse ID. PBSA was removed, and each sample was placed between two sponges in each cassette. All cassettes containing the samples were submerged in 80% (v/v) ethanol for up to one week until processing. Tissue processing was performed using an automated tissue processor (Excelsior ES Tissue Processor, Thermo Fisher Scientific), which follows 6 cycles of ethanol, 3 cycles of xylene, and 3 cycles of paraffin. Following tissue processing, all cassettes were opened, and samples were embedded in paraffin wax using the Thermo Fisher Histostar Tissue Embedding Station (Thermo Fisher Scientific) for sectioning on a microtome (Epredia Microtome HM 325, Thermo Fisher Scientific). The microtome was set to cut 10-µm thick tissue sections; they were first unfolded in a tissue section bath set at 30 °C–40 °C and then placed on microscope glass slides.[17]

2.7.2. De-paraffinization, rehydration, and staining of tissue sections

The slides with the tissue sections were placed in a 55 °C oven for 10 min to melt the paraffin. Then, all the slides were placed on a rack for de-paraffinization and rehydration via several washes in xylene and ethanol. At the end of the de-paraffinization process, the slides were washed in distilled water and placed on a rack.

Tissue sections were stained using Harris Hematoxylin Nuclear Stains (Leica Biosystems, Germany) and Eosin Secondary-Counter Stains (Leica Biosystems) to mark the nuclei of cardiac muscle cells and the ECM,[27,28] while Masson's trichrome (Abcam, USA) and Picro-Sirius Red Stain kits (Abcam) were used to stain collagen and cardiac muscle fibers in the cardiac tissue.[29-32] Hematoxylin and eosin (H&E) staining was performed through an automated tissue-staining machine (Thermo Shandon Varistain Gemini ES, Thermo Fisher Scientific). Masson's trichrome and Picro-Sirius red staining were performed according to the manufacturer's protocols.[17]

2.7.3. Sample preparation for tissue imaging and analysis of fibrosis

At the end of each staining, all slides were placed in a chemical fume hood to dry, and then DPX Neutral Mounting Medium (LABCHEM, Thermo Fisher Scientific) was applied to each sample. Once mounted, glass coverslips were placed on each sample and left to dry

before the edges were sealed with nail polish to prevent further drying. Samples were then imaged using ZEN 2.6 software on an Axio Scan.Z1 microscope (Zeiss, Germany) at 20× magnification, and each tissue staining was assessed using the LabKit plugin in ImageJ (Fiji) software (National Institutes of Health, USA). Samples were also imaged using an Olympus BX61 Upright fluorescence microscope (Japan) at 20× magnification. The analysis of the fibrotic tissue percentage ($n \geq 4$/group) was performed in Microsoft Excel (USA) on Masson's trichrome and Picro-Sirius red staining data using **Equation 1**:

$$Fibrotic\ tissue\ Percentage(\%) = \frac{Total\ fibrotic\ tissue\ area\ (\mu m^2)}{Total\ tissue\ area\ (\mu m^2)} \times 100 \quad (1)$$

where total tissue area represents both the fibrotic and non-fibrotic (healthy) areas of the tissue.[17]

2.8. RNA-sequencing analyses

Cardiac apex cryosections for euthanized mice were processed for messenger RNA (mRNA) transcriptomic analysis according to the protocol for the RNeasy® Fibrous Tissue Mini Kit (Qiagen, Germany).[17] Total RNA from each cardiac section was isolated by adding 14.3 M β-mercaptoethanol (β-ME) (Sigma-Aldrich) to the samples and purified according to the manufacturer's instructions. The lysate concentration was then calculated using a NanoDrop Microvolume Spectrophotometer (Thermo Fisher Scientific). Mouse RNA samples ($n \geq 3$/group) were then independently processed by BGI Genomics (Batch no. INSP21000010163, Hong Kong), and RNA quality assessment, library preparation, and sequencing were performed using DNBSEQ Eukaryotic Strand-specific mRNA libraries technology. Raw sequencing reads were filtered to include adapter sequences—more than 25% of bases matched an adapter sequence. Reads meeting the following four quality criteria were removed: (i) reads shorter than 150 bps, (ii) reads with more than 0.1% N, (iii) reads with more than 50 bps of polyX (X = A, T, G, C), and (iv) reads with more than 40% of bases having low quality (base quality < 20). The resultant high-quality reads were aligned to the mouse genome (mm10) through the STAR 2.7.11b (Spliced Transcripts Alignment to a Reference) software[33] with standard parameters. An average of 23,603,986 reads per sample was mapped, achieving an average alignment rate of 98.52%. The featureCounts tool was used to quantify gene expression levels.[34] Genes with fewer than 100 reads across the samples were excluded, reducing the gene count from 26,214 to 13,058. Expression levels were normalized using the DeSeq2 software package[35] in the R 4.4.1 statistical analysis software.[36] Genome-wide expression profiles were analyzed through MATLAB R2024a (MathWorks, USA) software's principal component analysis (PCA). Hierarchical clustering with complete linkage and Euclidean distance was performed using the pheatmap tool in the R statistical analysis software. The selected target genes were imported into Qiagen Ingenuity Pathway Analysis (IPA) and analyzed using the IPA Core Analysis algorithm.

2.9. Statistical analyses

Results were plotted in GraphPad Prism™ (USA), and the statistical significance of the analyses was assessed using a Brown–Forsythe and Welch ANOVA test, together with a Dunnett's T3 multiple comparisons test. US data were analyzed using a two-way ANOVA test with Tukey's multiple comparisons test, and results are represented as either mean ± SEM or the median value. Fibrosis data are represented as mean ± SEM, while hypertrophy data are shown as median. A p value of <0.05 was considered statistically significant.

3. Results

3.1. AlgGelSF patches are elastic and stretchable

To evaluate the potential protective effects of AlgGelSF patches against myocardial damage, they were implanted in an MI mouse model (Figure 1). First, AlgGel and AlgGelSF patches were printed as previously described (Section 2.3, Videos S1, S5, and S6), cut into smaller square pieces (Figure 2), and measured using a caliper to confirm their thickness (Figure S2). As AlgGel hydrogels are less viscous compared to the AlgGelSF-containing ones, as demonstrated in our previous studies,[9] AlgGel patches were slightly thinner than AlgGelSF patches, as shown in Figure S2A and S2B, respectively. However, both AlgGel and AlgGelSF patches were higher than the two-layer height set in the 3D bioprinter software, and their sizes were 4 mm × 4 mm × 2 mm. Both patch formulations could be manipulated and placed accurately over the heart (Figure 3 and Video S4).

AlgGelSF patches exhibited superior handling characteristics compared to AlgGel patches (Figure S1A–D). When the 20 mm × 20 mm × 2 mm patches were lifted from the well plate using a thin spatula (Figure S1A and S1C), the AlgGel patches displayed a gel-like behavior, folding around the spatula (Figure S1A) and showing a tendency to break. Conversely, the AlgGelSF patches exhibited greater elasticity, demonstrating resistance to curvature without breaking (Figure S1C). This flexibility was further evident when the patches were grasped and compressed between the fingers; after repeated movements and squeezing, the AlgGel patches tended to break (Figure S1B), whereas the AlgGelSF patches remained intact (Figure S1D).

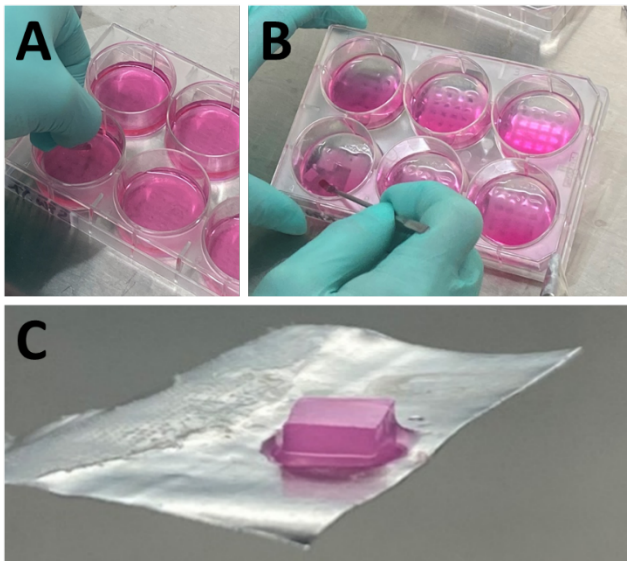


Figure 2. Patch preparation for *in vivo* transplantation. 3D-printed AlgGel and AlgGelSF patches cultured in cell culture medium (A) and cut into smaller pieces (B). Cut patches on sterile aluminum foil prior to transfer (C).
Abbreviations: Alg: Alginate; Gel: Gelatin; SF: Silk fibroin.

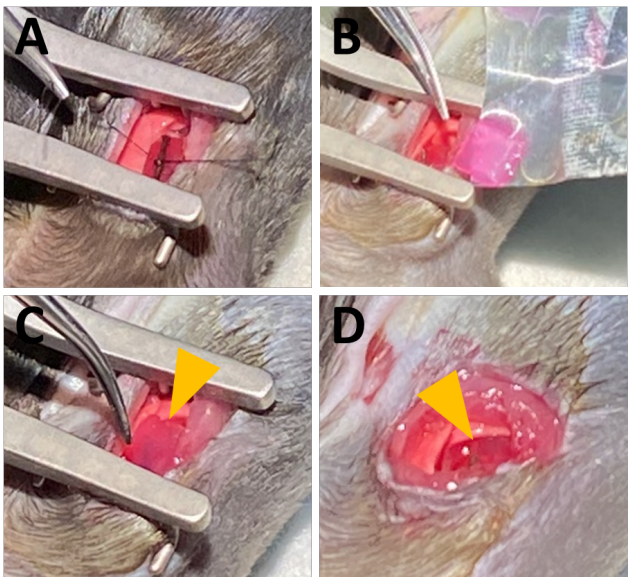


Figure 3. Myocardial infarction (MI)-induction surgery and 3D-printed patches transplantation. (A–D) The images represent a visual narrative of the sequential steps involved in the MI surgical procedure and subsequent transplantation of either AlgGel or AlgGelSF patches onto the MI site. Initially, the induction of MI is executed through the meticulous ligation of the left anterior descending (LAD) artery, accompanied by the strategic placement of a suture on the infarcted site (A). Subsequently, the 3D patch is transferred to the MI site (B) and precisely positioned onto the still-beating mouse heart using tweezers, as indicated by the yellow arrowhead (C). Successful integration of the 3D patch is indicated by its secure retention at the MI site. Finally, the mouse's chest is carefully sewn to complete the procedure, ensuring the stability and permanence of the transplanted patch on the infarcted region, as indicated by the yellow arrowhead (D). These images collectively illustrate the intricate and successful execution of the MI surgical procedure and 3D patch transplantation, showcasing the precision and efficacy of the experimental protocol.
Abbreviations: Alg: Alginate; Gel: Gelatin; SF: Silk fibroin.

In addition, tensile-strength tests were performed to mimic the mechanical stretch typical of healthy human cardiac tissue (Figure S1E–F and Videos S2 and S3). Over 24 hours, the stretchability of the AlgGelSF patch was monitored, and no rupture in the hydrogel structure was observed (Figure S1F), while partial degradation was already visible in the AlgGel patch after 3 h of testing (Figure S1E).

3.2. AlgGelSF patches protect against the reduction in cardiac function in infarcted mice

To evaluate the potential of AlgGelSF patches in improving the LVEF of myocardial infarcted mice, these patches were first implanted on the infarcted area, and echocardiography was performed (Figures 4 and S3). For each US measurement, both diastole (Figure 4A) and systole (Figure 4B) cycles were recorded. As expected, all experimental groups (*i.e.*, sham, MI, MI + AlgGel patch, and MI + AlgGelSF patch) did not present any significant difference in cardiac function at baseline (Figure 4C). Fourteen days post-surgery (Figure 4D), the MI group (37.49 ± 4.64%) showed a reduced LVEF of approximately 24 percentage points compared with the sham group (60.95 ± 3.52%), whereas the MI + AlgGel patch group (52.28 ± 4.56%) and the MI + AlgGelSF patch group (59.05 ± 3.60%) showed about 15 and 22 percentage points higher LVEF, respectively, compared with the MI group. At the endpoint (28 days post-surgery; Figure 4E), the LVEF of the MI + AlgGelSF patch group (59.64 ± 3.72%) was approximately 21 percentage points higher compared with the MI group (39.07 ± 3.02%), while that of the MI + AlgGel patch group (49.51 ± 2.85%) was about 10 percentage points higher compared with the MI group. The significant difference in LVEF between the two patch groups was approximately 10 percentage points. In contrast, no significant difference was detected between the sham group and the MI + AlgGelSF patch group, indicating that the AlgGelSF patches recover cardiac functions to a level comparable to that in sham mice (61.82 ± 4.18%; Figure 4F).

3.3. Myocardial infarction models do not lead to hypertrophic tissue formation

To evaluate cardiac hypertrophy after MI, heart weight was normalized to body weight and/or tibia length. Assuming that myocardial remodeling leads to an increase in scar tissue in the myocardial wall, there should also be an increase in heart weight, while the tibia length remains unchanged. Figure S3 shows no measurable hypertrophy across all groups, as evidenced by the lack of significant differences in heart weight/body weight ratios (mean values between 0.004 and 0.009) and heart weight/tibia length ratios (mean values between 7 and 11 mg/mm).

3.4. AlgGelSF patches protect against fibrosis in the myocardial infarction model

To assess the amount of fibrotic tissue generated after MI, and to measure the accumulation of heart muscle fiber within the cardiac tissue post-MI, H&E, Masson's trichrome, and Picro-Sirius red staining were performed. As shown in Figures 5A and S4A, cardiac muscle fibers in the sham group exhibited a straight-line pattern, consistent with proper function. For the MI group (Figures 5B, S4B, and S5B), muscle fibers were only partially aligned, while cells and ECM were disorganized. The muscle fibers of the MI + AlgGel patch group tended to align (Figures S4C & S5C). Of note, the MI + AlgGelSF patch group displayed a fiber alignment similar to that of the sham group (Figures 5D, S4D, & S5D).

Masson's trichrome staining (Figure 5A–D) was used to identify connective tissues and to evaluate fibrosis, visualizing the distribution of collagen fibers in murine cardiac tissues post-MI. Cardiac muscle fibers were stained in purple, whereas collagen fibers were stained in blue.[31,32] Figure 5E shows the percentages of fibrotic tissue in all groups, calculated according to **Equation 1**. The sham group presents aligned collagen fibers (Figure 5A) and a minor area of fibrotic tissue (3.99 ± 2.51%). The MI group (Figure 5B) shows partial organization of muscle fibers and a larger fibrotic region with a higher collagen fiber density (13.22 ± 7.05%), approximately 9 percentage points higher than the sham group. The MI + AlgGel patch group (10.68 ± 6.79%; Figure 5C) showed a decrease in the fibrotic area, with the muscle fibers tending to be more aligned, even though the fibrotic tissue percentage was approximately 3 percentage points less compared with the MI group. The MI + AlgGelSF patch group (5.42 ± 4.93%; Figure 5D) showed more aligned muscle fibers and a lower density of collagen fibers, approximately 5 percentage points less compared with the MI + AlgGel patch group and approximately 8 percentage points less than the MI group. The fibrotic tissue percentage of the MI + AlgGelSF patch group was similar to that of the sham group, with no significant difference.

Picro-Sirius red staining (Figure S5) was used as a complementary method to stain collagen fibers, with cardiac muscle fibers stained in yellow, and collagen fibers in red.[29,30] Cardiac muscle fibers were aligned and well-organized in the sham group (Figure S5A), whereas the MI group (Figure S5B) presented a partial muscle fiber alignment and disorganization of the collagen fibers. The MI group also showed a higher collagen fiber density and a larger fibrotic region. A decrease in the fibrotic tissue percentage in the MI + AlgGel patch group (Figure S5C) was observed. Furthermore, the collagen fibers and muscle

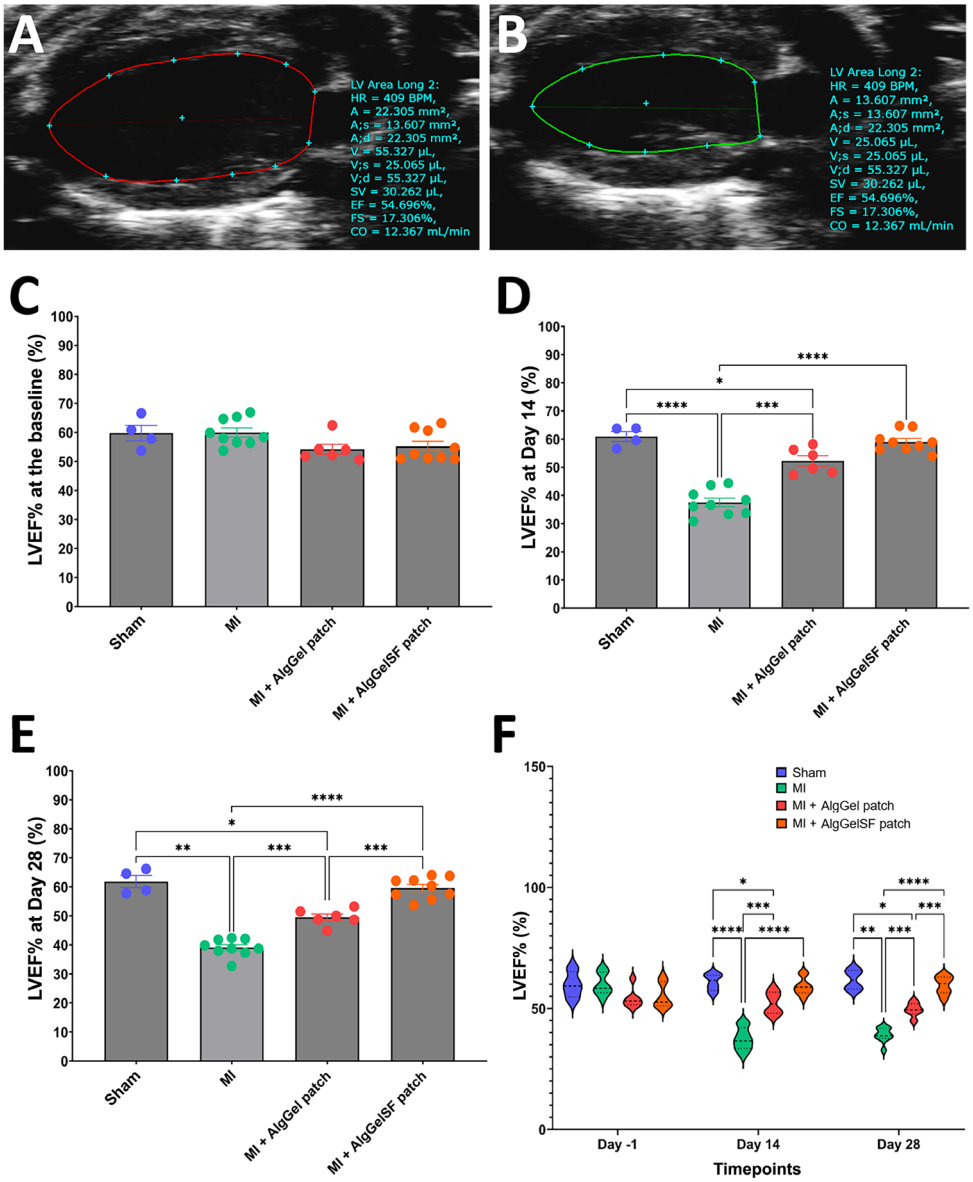


Figure 4. AlgGelSF patches improve the left ventricular ejection fraction (LVEF) of murine hearts post-MI. (A–B) The images are representative of murine parasternal long-axis US images analyzed using VevoLAB software, acquired from the MI + AlgGelSF patch group. Both the diastolic (A) and systolic (B) cycles are outlined in the manual and automatic (AutoLV) modes. The software also shows data relative to: heart rate (HR; bpm), area of the cycle (A; mm^2), area of systole (A; s; mm^2), area of diastole (A; d; mm^2), volume of the cycle (V; µL), volume of systole (V; s; µL), volume of diastole (V; d; µL), stroke volume (SV; µL), LVEF (EF; %), fractional shortening (FS; %), and cardiac output (CO; mL/min). (C–E) The plots show LVEF analyses from US data acquired in parasternal long-axis view using the Vevo 3100 Preclinical Imaging System. The LVEFs were analyzed at baseline (1 day before surgery) (C), Day 14 (midpoint) (D), and Day 28 (endpoint) (E). US data were analyzed using the Vevo LAB 5.7.1 software, and Brown–Forsythe and Welch ANOVA tests, together with a Dunnett's T3 multiple comparisons test, were performed. Data are presented as means ± SEM. (F) Representative of LVEFs from all experimental groups across all three time points (baseline [Day −1], midpoint [Day 14], endpoint [Day 28]). A two-way ANOVA with Tukey's multiple comparisons test was performed, and data are presented as median with 25% and 75% interquartile ranges.
Notes: $n \geq 4$/group; $^{*}p < 0.05$, $^{**}p < 0.01$, $^{***}p < 0.001$, $^{****}p < 0.0001$.
Abbreviations: Alg: Alginate; Gel: Gelatin; MI: Myocardial infarction; SF: Silk fibroin; US: Ultrasound.

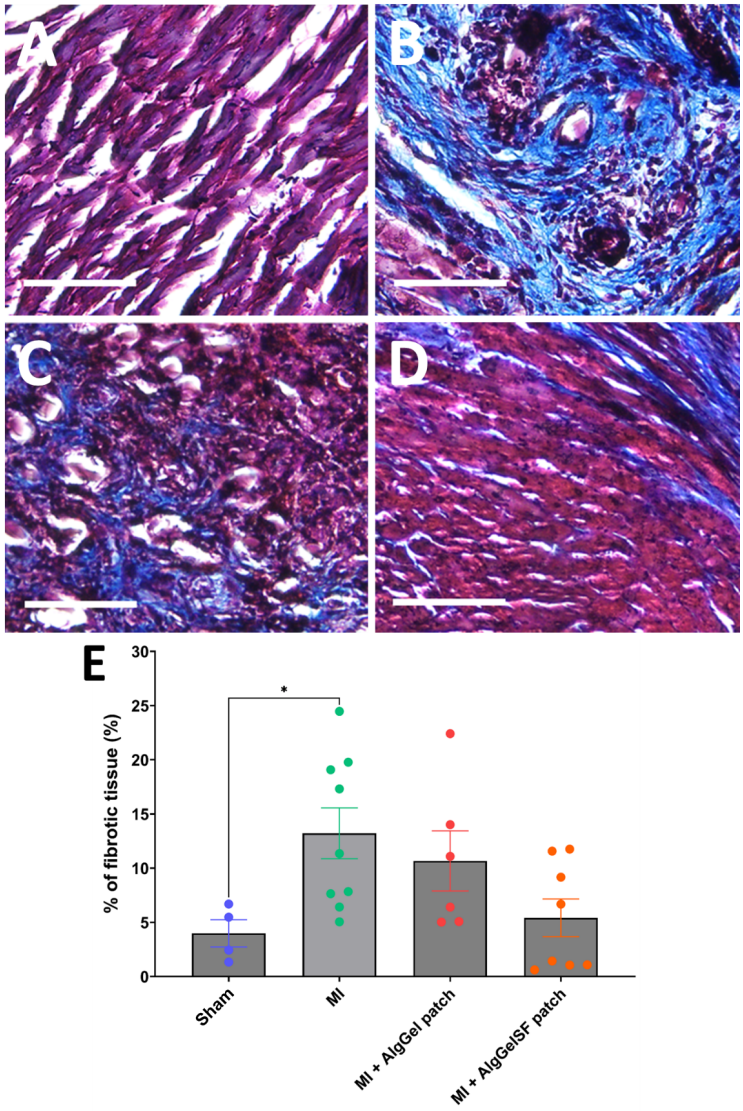


Figure 5. Masson's trichrome staining and analysis of fibrotic tissue percentage. (A–D) Representative images of Masson's trichrome staining acquired through Olympus BX61 upright fluorescence microscope: sham (A), MI (B), MI + AlgGel patch (C), and MI + AlgGelSF patch (D). Collagen fibers are stained in blue and cardiac muscle fibers in purple (scale bars: 100 μm; magnifications: 20×). (E) The plot represents the analysis of fibrotic tissue percentages across all experimental groups. It shows an increase in fibrotic tissue percentage in the MI group, followed by a progressive decrease in the MI + AlgGel patch and MI + AlgGelSF patch groups. The statistical analysis was performed using the Brown–Forsythe and Welch ANOVA tests, with Dunnett's T3 multiple comparisons test. Data are presented as mean ± SEM.
Notes: n≥4/group; $^*p < 0.05$.
Abbreviations: Alg: Alginate; Gel: Gelatin; MI: Myocardial infarction; SF: Silk fibroin.

fibers tended to re-align. The MI + AlgGelSF patch group (Figure S5D) showed aligned muscle and collagen fibers and less fibrotic tissue deposition.

3.5. AlgGelSF patches promote the expression of genes regulating cardiac remodeling in myocardial infarcted mice

Bulk RNA sequencing on the experimental animals was performed to evaluate their transcriptomes and analyze the expression of specific gene sequences involved in cardiac remodeling after MI.[37,38] RNA isolation and sequencing were performed for the following animal experimental groups: sham, MI, MI + AlgGel patch, and MI + AlgGelSF patch.[17]

The PCA explains the variability in gene expression.[39] The PCA plot (Figure 6A) represents the genome-wide

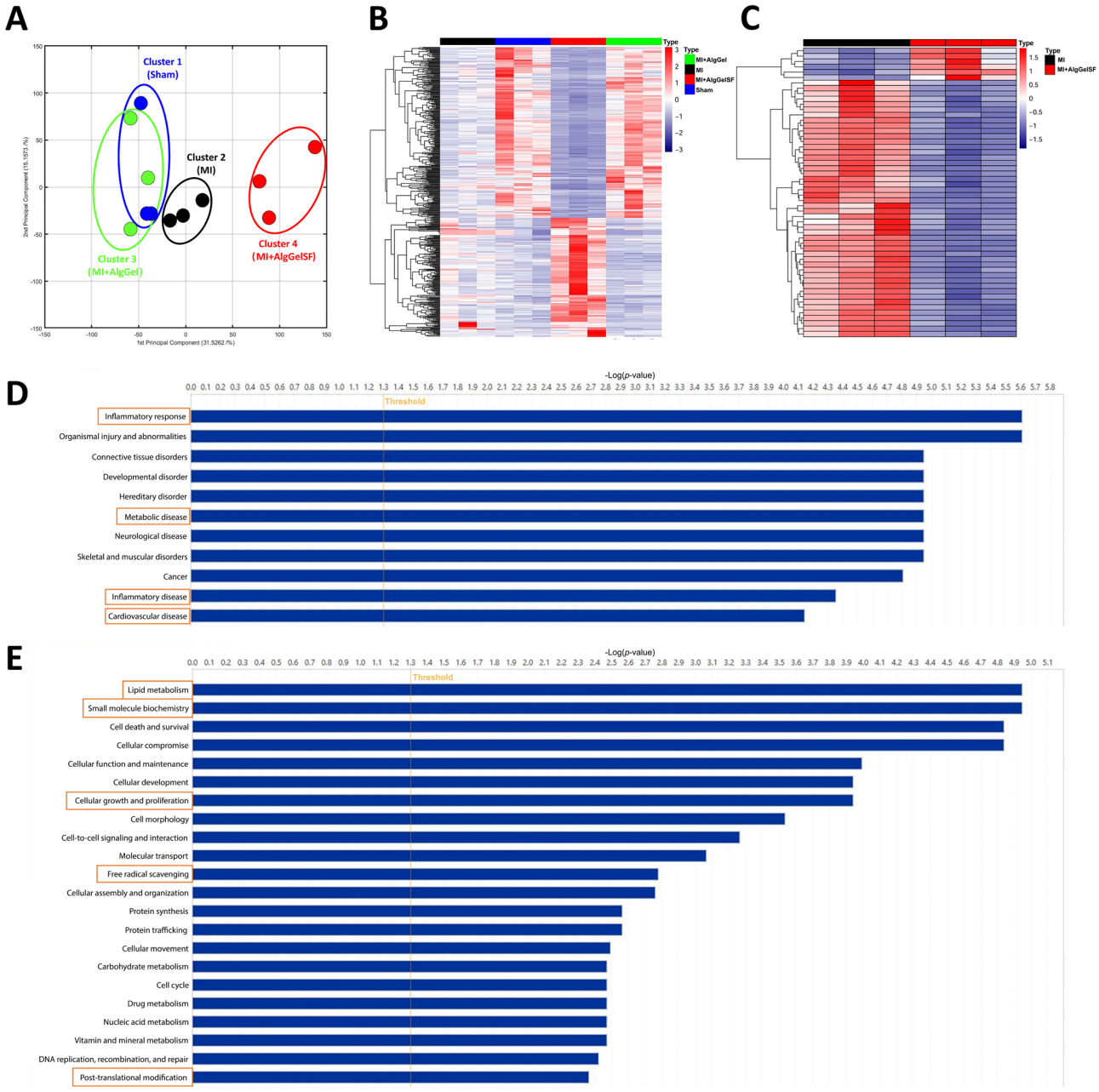


Figure 6. Transcriptomic profiles. (A–E) Representative images derived from RNA sequencing analysis performed on experimental groups: sham, MI, MI + AlgGel patch, and MI + AlgGelSF patch. (A) The image represents the principal component analysis (PCA) of the whole transcriptomic profile. (B–C) The two heatmaps show the gene expression levels of differentially expressed genes across all groups (B) and between the MI and MI + AlgGelSF patch groups (C). (D–E) Representative images of the enrichment analysis for differentially expressed genes between the MI and MI + AlgGelSF patch groups: diseases (D) and molecular and cellular functions (F).
Notes: $n \geq 3$; fold change > 1.5 and < −1.5; $\alpha = 0.05$.
Abbreviations: Alg: Alginate; Gel: Gelatin; MI: Myocardial infarction; SF: Silk fibroin

expression profiles of the samples and was characterized by two principal components (PCs). The first PC accounted for the primary difference in gene expression across the four experimental groups, explaining 31.53% of the variance. The second PC accounted for the secondary variation in gene expression, due to individual sample variability, explaining 15.16% of the variance. Both PCs accounted for 46.69% of the total variance in the dataset. Sham samples showed consistent gene expression profiles, whereas MI samples displayed a distinct profile. Figure 6A reveals distinct clustering patterns, indicating a substantial gene expression difference across the four experimental groups: Cluster 1 represents the sham (control) group, Cluster 2 represents the MI group, Cluster 3 represents the MI + AlgGel patch group, and Cluster 4 represents the MI + AlgGelSF patch group. Cluster 4 was well-separated from Cluster 2, suggesting that the MI + AlgGelSF patch induces a significant shift in gene expression compared to the MI samples. Samples from Clusters 1 and 2 shared similarities in their gene expression profiles.

The differential gene expression analysis identified 168 transcripts across the four experimental mouse groups, using cut-off criteria of a fold change (FC)> 1.5 or < −1.5 and a *p*-value of 0.05. The analysis included upregulated and downregulated genes; an FC > 1.5 indicates upregulation, while an FC < −1.5 indicates downregulation.[40] The variations in gene expression driven by molecular responses pre- and post-MI are presented in the heatmaps in Figure 6B–C.[41] Our hierarchical clustering analysis of the murine transcripts showed clear gene expression patterns of upregulation (red) and downregulation (blue). Figure 6B reveals distinct transcriptional changes that differ across the four groups. Figure 6C directly compares more refined gene expression patterns between the MI group and the MI + AlgGelSF patch group. The Ingenuity Pathway Analysis (IPA; Figure 6D–E) comparing the MI group and the MI + AlgGelSF patch group highlighted the enrichment of genes associated with specific post-MI pathways in the MI + AlgGelSF patch group.[42,43] Table 1 presents the top 64 transcripts that were differentially expressed in the MI + AlgGelSF patch group. These transcripts indicate enrichment across specific categories, such as inflammatory response and disease, metabolic disease, lipid metabolism, and redox signaling. IPA also identified upregulated and downregulated genes involved in cardiac tissue remodeling and fibrosis post-MI, such as *COL4A5* and *COL5A2*, as well as in the inflammatory response and cellular growth and proliferation, including *BMI1*, *CD247*, *CD52*, *GNA12*, *NCOA4*, *PPARGC1A*, *TREM2*, *TXN*, and *TYROBP*. Genes such as *BMI1*, *CD247*, *COL4A5*, *COL5A2*, *GNA12*, *NCOA4*, and *PPARGC1A* were upregulated, while *CD52*, *TREM2*, *TXN*, and *TYROBP* were downregulated (Table 2).

4. Discussion

This study describes the effects of 3D-bioprinted cell-free AlgGelSF patch transplantation into an MI murine model to assess the potential cardioprotective effects. Overall, these patches protected against MI-induced reductions in LVEF and fibrosis, and modulated genes involved in key myocardial disease mechanisms.

The transplantation of 3D-printed AlgGelSF patches into the MI mouse model yielded promising results, showing the effectiveness of the surgical procedure. This success may be attributed to the tensile strength (Figure S1E–F) and elastic properties of AlgGelSF-containing materials, which provide greater resistance to deformation and improve handling abilities (Figure S1A–D). Tensile-strength testing also revealed the exceptional stretchability of AlgGelSF patches, demonstrating SF's ability to adapt and withstand deformation during cardiac tissue contraction (Figure S1F).[2,9,19]

The elastic properties of SF may allow the 3D-printed patch to adjust to and better adapt to the irregularities of the cardiac tissue microenvironment without compromising its structural integrity.[44-46] Our qualitative analyses showed improved handling of the AlgGelSF patches, resulting in enhanced surgical precision during patch placement compared with the AlgGel patches (Videos S5 & S6, respectively).

We previously demonstrated that increasing SF concentrations in AlgGel formulations improved the structural and mechanical properties of AlgGel hydrogels and enhanced their durability in physiological environments.[9] This improvement was attributed to the presence of β-sheets in the crosslinked 3D-printed patches, which strengthen hydrogen bonding within the SF structure and delay the degradation of AlgGel hydrogels, which typically degrade more rapidly in physiological environments.[9] The enhanced mechanical stability of AlgGelSF patches may result from strengthened hydrogen bonding and electrostatic interactions.[9] In addition, the presence of RGD sequences (from Gel) promotes interactions with cell-surface integrin receptors, which may additionally support adhesion of the patch to the heart.[47-50]

The absence of detectable cardiac hypertrophy following transplantation of both AlgGel and AlgGelSF patches (Figure S3) was an interesting finding, as cardiac hypertrophy can lead to HF and other pathological complications.[51] The lack of hypertrophic responses in the

Table 1. Ingenuity Pathway Analysis of differentially expressed genes associated with disease and molecular and cellular functions in the MI and MI + AlgGelSF patch groups

Category	*p*-value	mRNAs
Inflammatory response	2.45E−6–3.37E−2	*Anxa9*, *Atp2b1*, *Bmi1*, *Cd247*, *Cd300a*, *Cd52*, *Ckb*, *Cog5*, *Col4a5*, *Col5a2*, *Ctsz*, *Dsg2*, *Fam227b*, *Fau*, *Ftl*, *Gadd45b*, *Gna12*, *Hba2*, *Hbb-b2*, *Il27*, *Itpkb*, *Klhl24*, Mir142 (includes others), *Msmp*, *Mt1*, *Ncoa4*, *Nt5dc2*, *Pltp*, *Pmel*, *Ppargc1a*, *Psmb9*, *Pus10*, *Renbp*, *Rmc1*, *S100a6*, *Sh3bgrl3*, *Syt6*, *Tgif1*, *Tmem179*, *Tmsb10*, *Tob1*, *Tpm3*, *Trem2*, *Txn*, *Tyrobp*, *Usp9x*
Metabolic disease	1.13E−5–2.72E−2	*C18orf32*, *Cd247*, *Cd300a*, *Cd52*, *Ckb*, *Cog5*, *Col12a1*, *Col4a5*, *Col5a2*, *Cstb*, *Ctsz*, *Dnah11*, *Dsg2*, *Eif2s3*, *Fam227b*, *Ftl*, *Gadd45b*, *Gm15350*, *Gpld1*, *Hba2*, *Hbb-b2*, *Itpkb*, Mir142 (includes others), *Mt1*, *Ncoa4*, *Nelfcd*, *Pigf*, *Pltp*, *Ppargc1a*, *Psmb9*, *Pus10*, *Rmc1*, *S100a6*, *Sfi1*, *Tgif1*, *Tmem205*, *Tmsb10*, *Tpm3*, *Trem2*, *Txn*, *Tyrobp*
Inflammatory disease	4.43E−5–3.01E−2	*Anxa9*, *Atp2b1*, *Bmi1*, *Cd247*, *Cd52*, *Ckb*, *Cog5*, *Col4a5*, *Col5a2*, *Ctsz*, *Fam227b*, *Fau*, *Ftl*, *Gadd45b*, *Gna12*, *Hba2*, *Hbb-b2*, *Il27*, *Itpkb*, *Klhl24*, Mir142 (includes others), *Mt1*, *Ncoa4*, *Nt5dc2*, *Pltp*, *Pmel*, *Ppargc1a*, *Psmb9*, *Pus10*, *Renbp*, *Rmc1*, *S100a6*, *Sh3bgrl3*, *Stmn1*, *Syt6*, *Tgif1*, *Tmem179*, *Tmsb10*, *Tob1*, *Tpm3*, *Trem2*, *Txn*, *Tyrobp*
Cardiovascular disease	7.21E−5–3.01E−2	*Bmi1*, *Cd52*, *Col4a5*, *Col5a2*, *Dnah11*, *Dsg2*, *Ftl*, *Gdf1*, *Hba2*, *Hbb-b2*, *Il3ra*, *Klhl24*, *Ncoa4*, *Pltp*, *Ppargc1a*, *Stmn1*, *Tgif1*, *Tmem205*, *Trem2*, *Txn*, *Tyrobp*, *Usp9x*
Lipid metabolism	1.13E−5–3.33E−2	*Gna12*, *Gpld1*, *Itpkb*, *Ncoa4*, *Pltp*, *Ppargc1a*, *Stmn1*, *Tmem150a*, *Trem2*, *Tyrobp*
Small molecule biochemistry	1.13E−5–3.33E−2	*Atp2b1*, *Ckb*, *Eif2s3*, *Ftl*, *Gna12*, *Gpld1*, *Hba2*, *Hbb-b2*, *Itpkb*, *Mt1*, *Ncoa4*, *Nt5c*, *Pltp*, *Ppargc1a*, *Renbp*, *Stmn1*, *Tmem150a*, *Trem2*, *Txn*, *Tyrobp*
Cellular growth and proliferation	1.15E−4–3.37E−2	*Bmi1*, *Cd247*, *Cd300a*, *Cd52*, *Col12a1*, *Ctsz*, *Dsg2*, *Ftl*, *Gadd45b*, *Gna12*, *Hbb-b2*, *Il27*, *Itpkb*, Mir142 (includes others), *Mt1*, *Ncoa4*, *Pigf*, *Pmel*, *Ppargc1a*, *Rmi1*, *S100a6*, *Stmn1*, *Tgif1*, *Tob1*, *Trem2*, *Txn*, *Tyrobp*, *Usp9x*
Free radical scavenging	1.67E−3–3.33E−2	*Bmi1*, *Cd52*, *Cstb*, *Ftl*, *Hba2*, *Hbb-b2*, *Ppargc1a*, *S100a6*, *Txn*, *Tyrobp*
Post-translational modification	4.33E−3–2.48E−2	*Ftl*, *Klhl24*, *Lrsam1*, *Txn*

Abbreviations: Alg: Alginate; Gel: Gelatin; MI: Myocardial infarction; mRNA: Messenger RNA; SF: Silk fibroin.

MI + AlgGelSF patch group suggests a potential beneficial interaction between the patch and native cardiac tissue, which warrants further investigation.

To evaluate cardiac function across all experimental groups and determine whether AlgGelSF patches improved cardiac function in MI mice, US data were analyzed for LVEF at specific time points (Figure 4C–F). The results demonstrated the efficacy of 3D-printed AlgGelSF patches in improving cardiac function (Figure S6). After 28 days of treatment, MI mice receiving AlgGelSF patches exhibited an approximately 10 percentage points higher LVEF than those receiving AlgGel patches and an approximately 20 percentage points higher LVEF than untreated MI mice. This improved LVEF level was not significantly different from that observed in healthy mice (sham group), demonstrating an improvement in cardiac function post-MI.[52,53]

The analysis of cardiac function was supported by histological analyses to evaluate collagen fiber deposition (expressed as the percentage of fibrotic tissue area) after MI. The MI + AlgGelSF patch group exhibited a lower percentage of fibrotic tissue in the infarct area compared with the MI group, with a level similar to that of the sham group. These results support a protective role of AlgGelSF patches against cardiac fibrosis.[44,52]

The improvement in cardiac function was also supported by the transcriptomic results. PCA of genome-wide expression profiles (Figure 6A) revealed a distinct cluster in the MI group, indicating a profound transcriptomic shift associated with ischemic injury. This finding was consistent with the US analysis performed after 28 days, which showed an approximately 23 percentage point reduction in LVEF compared with the sham group

Table 2. Ingenuity Pathway Analysis of upregulated and downregulated genes involved in cardiac tissue remodeling and fibrosis post-MI in the MI and MI + AlgGelSF patch groups

Gene	Log_2 fold change	*p*-value	Up- or downregulation
Bmi1	1.5753914870	0.000490710	Upregulation
Cd247	1.5831218730	0.000581403	Upregulation
Cd52	−1.5352729120	0.000908230	Downregulation
Ckb	−1.5331035860	0.000031300	Downregulation
Col4a5	1.6072523500	0.001040459	Upregulation
Col5a2	1.5879678500	7.75E−9	Upregulation
Ctsz	−1.6315919670	0.000016000	Downregulation
Dsg2	1.5229152520	0.001580242	Upregulation
Ftl1	−1.5666122130	0.000001590	Downregulation
Gadd45b	−2.0205187810	0.000005020	Downregulation
Gna12	2.0477009690	0.000001110	Upregulation
Hba-a2	−1.7163516810	0.000002690	Downregulation
Hbb-b2	−1.6093259680	0.000013400	Downregulation
Itpkb	1.6190159180	0.000767415	Upregulation
Klhl24	1.9647872410	0.000001120	Upregulation
Mir142b	−1.5807620800	0.003309117	Downregulation
Mt1	−1.6719987120	0.000000333	Downregulation
Ncoa4	1.7206685100	0.000245836	Upregulation
Pltp	−1.6874330890	0.000001470	Downregulation
Ppargc1a	1.7060340540	0.000279861	Upregulation
S100a6	−1.5125309040	0.000007010	Downregulation
Stmn1	−1.6374872650	0.000139962	Downregulation
Tgif1	−1.5006135260	0.005825072	Downregulation
Trem2	−2.0246321960	0.000003080	Downregulation
Txn1	−1.5530094380	0.000085900	Downregulation
Tyrobp	−1.5227029040	0.000160021	Downregulation

Abbreviations: Alg: Alginate; Gel: Gelatin; MI: Myocardial infarction; SF: Silk fibroin.

(Figure 4E–4F). Interestingly, the MI + AlgGelSF patch group clustered further away from both the MI and sham groups, suggesting that AlgGelSF treatment may induce additional molecular changes associated with improved cardiac function. In addition, gene expression results (Figure 6C) suggest that AlgGelSF patches may attenuate inflammatory and fibrotic responses while promoting pathways involved in cardiac tissue repair and limiting excessive collagen deposition during cardiac remodeling.[5,52]

We used degummed SF as an inert material to minimize potential immune responses associated with the implanted material. This consideration is critical for reducing potential complications in future human applications and supporting its long-term safety for cardiac tissue engineering.[54] However, enrichment analysis of differentially expressed genes (Figure 6D–E and Table 2) supported the role of AlgGelSF patches in modulating inflammatory responses and reducing cardiomyocyte loss, as indicated by the downregulation of *Cd52*, *Tyrobp*, *Stmn1*, and *Gadd45b*.[55-59] The enrichment analysis further suggested potential protective effects of SF through the upregulation of genes such as *Bmi1*, *Ppargc1a*, *Dsg2*, and *Klhl24*, which are involved in regulating cardiac tissue regeneration, lipid metabolism, or structural integrity.[60-63] Notably, the increased expression of *Cd247* and *Cd52* (Tables S1 and S2), which are expressed in natural killer (NK) and T cells, suggests a role for NK cell-mediated responses in the absence of T cells in *Rag1*-deficient mice. These genes were differentially expressed in the MI + AlgGelSF patch group but not in the MI + AlgGel patch group. This finding indicates involvement of an early immune defense response, which has been shown to play a protective role against cardiac fibrosis.[64] These transcriptomic results are consistent with our histological findings and support an inflammation-mediated protection against cardiac fibrosis and preservation of cardiac function.

However, our study has several limitations. While the acellular AlgGelSF patches enable assessment of biocompatibility and mechanical support for infarcted tissue, the absence of cells limits their ability to restore active myocardial function. Therefore, evaluating cell-laden patches is a critical next step to promote contractility, vascularization, and electromechanical coupling. In addition, although murine MI models are essential for initial *in vivo* evaluation, anatomical and physiological differences between murine and humans limit direct clinical extrapolation. Therefore, the effects of AlgGelSF patches on immunocompetent animal models should be evaluated to improve clinical translation. Further analyses of patch retention, degradation, and integration with host tissue during the 28-day implantation period will be critical for understanding *in vivo* performance. Additional SF concentrations should also be evaluated. Notably, infarct size was not quantified in this study, limiting the ability to correlate functional recovery with structural cardiac repair. Independent validation using quantitative polymerase chain reaction or immunohistochemical analyses will further validate our transcriptomic findings. Moreover, tensile-strength testing was limited to qualitative observations; quantitative measurements, such as tensile strength, elastic modulus, and elongation at break, will be critical to evaluate the performance of the printed hydrogel under dynamic conditions. Finally, progression to large-animal models, such as pigs, will enable evaluation using clinically relevant patch sizes and surgical techniques that better reflect human cardiac anatomy and biomechanics. Successful validation in these models will be pivotal for advancing 3D-bioprinted AlgGelSF-based cardiac patches toward clinical application.

Future work should focus on formulating AlgGelSF-containing bioinks incorporating cardiac spheroids composed of cardiomyocytes, endothelial cells, and cardiac fibroblasts. These spheroids may proliferate and fuse after printing, better recapitulating the native 3D cardiac microenvironment and enhancing functional integration with the host myocardium.[17,65]

5. Conclusion

The 3D-printed AlgGelSF patches protect against post-MI deterioration of cardiac function by improving LVEF, reducing cardiac fibrosis, and modulating the expression of genes regulating immune responses. Altogether, these findings support the potential of AlgGelSF-containing hydrogels as a promising approach for cardiac protection *in vivo*.

Acknowledgments

We would like to thank Dr. Shripad Bangale from VisualSonics (FUJIFILM Asia Pacific Pte Ltd, Singapore) for the support with the ultrasound machine. We also want to thank Assoc/Prof. Louise Cole for assisting during imaging at the Microbial Imaging Facility (University of Technology Sydney) and Dr. Veronika Valova for supporting us in analyzing histology images.

Funding

The University of Technology Sydney supported Dr. Laura Vettori with the International Research Scholarship and UTS President's Scholarships. Dr. Ashton Matthee was supported by a Heart Research Institute Fellowship.

Associate Prof. Carmine Gentile was supported by a UTS Seed Funding, a Heart Research Australia Grant, a 2022, a 2023, a 2024, a 2025, and a 2026 Perpetual IMPACT Grant, and a Catholic Archdiocese of Sydney Grant for Adult Stem Cell Research. Dr. Hien A. Tran was supported by the Vingroup Science and Technology Scholarship Program.

Conflict of interest

The authors declare they have no competing interests.

Author contributions

Conceptualization: Laura Vettori, Carmine Gentile
Formal analysis: Laura Vettori
Investigation: Laura Vettori
Methodology: Laura Vettori, Clara Liu Chung Ming, Niina Matthews, Dominick Beck, Timothy Couttas, Hien Ahn Tran
Writing–original draft: Laura Vettori
Writing–review & editing: Carmine Gentile, Ashton Matthee, Jelena Rnjak-Kovacina

Ethics approval and consent to participate

All procedures were approved by the Animal Ethics Committee at the University of Technology Sydney (ETH19-4338).

Consent for publication

Not applicable.

Availability of data

Data are available from the corresponding author upon reasonable request.

Further disclosure

Part of or the entire set of findings have been presented in a conference, academic seminars and meetings.

References

1. Wang Y, Wang C, Shen L, Xu D. The Role of Regulatory T Cells in Heart Repair After Myocardial Infarction. *J Cardiovasc Transl Res*. 2023;16(3):590-597.

   doi: 10.1007/s12265-022-10290-5

2. Liu T, Hao Y, Zhang Z, *et al*. Advanced Cardiac Patches for the Treatment of Myocardial Infarction. *Circulation*. 2024;149(25):2002-2020.

   doi: 10.1161/CIRCULATIONAHA.123.067097

3. Sharma P, Wang X, Ming CLC, *et al*. Considerations for the Bioengineering of Advanced Cardiac In Vitro Models of Myocardial Infarction. *Small*. 2021;17(15):e2003765.

   doi: 10.1002/smll.202003765

4. Vettori L, Sharma P, Rnjak-Kovacina J, Gentile C. 3D Bioprinting of Cardiovascular Tissues for In Vivo and In Vitro Applications Using Hybrid Hydrogels Containing Silk Fibroin: State of the Art and Challenges. *Curr Tissue Microenviron Rep*. 2020;1(4):261-276.

   doi: 10.1007/s43152-020-00026-5

5. Chen R, Zhang H, Tang B, *et al*. Macrophages in cardiovascular diseases: molecular mechanisms and therapeutic targets. *Signal Transduct Target Ther*. 2024;9(1):130.

   doi: 10.1038/s41392-024-01840-1

6. Frangogiannis NG. Cardiac fibrosis: Cell biological mechanisms, molecular pathways and therapeutic opportunities. *Mol Aspects Med*. 2019;65:70-99.

   doi: 10.1016/j.mam.2018.07.001

7. Raziyeva K, Kim Y, Zharkinbekov Z, Temirkhanova K, Saparov A. Novel Therapies for the Treatment of Cardiac Fibrosis Following Myocardial Infarction. *Biomedicines*. 2022;10(9):2178.

   doi: 10.3390/biomedicines10092178

8. Yin X, Yin X, Pan X, *et al*. Post-myocardial infarction fibrosis: Pathophysiology, examination, and intervention. *Front Pharmacol*. 2023;14:1070973.

   doi: 10.3389/fphar.2023.1070973

9. Vettori L, Tran HA, Mahmodi H, *et al*. Silk fibroin increases the elasticity of alginate-gelatin hydrogels and regulates cardiac cell contractile function in cardiac bioinks. *Biofabrication*. 2024;16(3):035025.

   doi: 10.1088/1758-5090/ad4f1b

10. Chen J, Zhan Y, Wang Y, *et al*. Chitosan/silk fibroin modified nanofibrous patches with mesenchymal stem cells prevent heart remodeling post-myocardial infarction in rats. *Acta Biomater*. 2018;80:154-168.

    doi: 10.1016/j.actbio.2018.09.013

11. de Winter N, Ji J, Sintou A, *et al*. Persistent transcriptional changes in cardiac adaptive immune cells following myocardial infarction: New evidence from the re-analysis of publicly available single cell and nuclei RNA-sequencing data sets. *J Mol Cell Cardiol*. 2024;192:48-64.

    doi: 10.1016/j.yjmcc.2024.04.016

12. Polonchuk L, Surija L, Lee MH, *et al*. Towards engineering heart tissues from bioprinted cardiac spheroids. *Biofabrication*. 2021;13(4):045009.

    doi: 10.1088/1758-5090/ac14ca

13. Roche CD, Sharma P, Ashton AW, Jackson C, Xue M, Gentile C. Printability, Durability, Contractility and Vascular Network Formation in 3D Bioprinted Cardiac Endothelial Cells Using Alginate-Gelatin Hydrogels. *Front Bioeng*

Biotechnol. 2021;9:636257.

doi: 10.3389/fbioe.2021.636257

14. Das P, Ganguly S, Marvi PK, *et al*. Carbon Dots Infused 3D Printed Cephalopod Mimetic Bactericidal and Antioxidant Hydrogel for Uniaxial Mechano-Fluorescent Tactile Sensor. *Adv Mater*. 2024;36(48):e2409819.

doi: 10.1002/adma.202409819

15. Panico A, Corvi A, Collini L, Sciancalepore C. Multi objective optimization of FDM 3D printing parameters set via design of experiments and machine learning algorithms. *Sci Rep*. 2025;15(1):16753.

doi: 10.1038/s41598-025-01016-z

16. Wang X, Liu X, Li K, *et al*. A Microgel-Hydrogel Hybrid for Functional Compensation and Mechanical Stability in 3D Printed Cell-Dense Vascularized Liver Tissue. *Adv Mater*. 2025;37(28):e2413940.

doi: 10.1002/adma.202413940

17. Roche CD, Lin H, Huang Y, *et al*. 3D bioprinted alginate-gelatin hydrogel patches containing cardiac spheroids recover heart function in a mouse model of myocardial infarction. *Bioprinting*. 2023;30:e00263.

doi: 10.1016/j.bprint.2023.e00263

18. Huang K, Ozpinar EW, Su T, *et al*. An off-the-shelf artificial cardiac patch improves cardiac repair after myocardial infarction in rats and pigs. *Sci Transl Med*. 2020;12(538):eaat9683.

doi: 10.1126/scitranslmed.aat9683

19. Tran HA, Hoang TT, Maraldo A, *et al*. Emerging silk fibroin materials and their applications: New functionality arising from innovations in silk crosslinking. *Mater Today*. 2023;65:244-259.

doi: 10.1016/j.mattod.2023.03.027

20. Giuseppe MD, Law N, Webb B, *et al*. Mechanical behaviour of alginate-gelatin hydrogels for 3D bioprinting. *J Mech Behav Biomed Mater*. 2018;79:150-157.

doi: 10.1016/j.jmbbm.2017.12.018

21. Kumaraswami K, Arnholdt C, Deindl E, Lasch M. Rag1 Deficiency Impairs Arteriogenesis in Mice. *Int J Mol Sci*. 2023;24(16):12839.

doi: 10.3390/ijms241612839

22. Cui X, Soliman BG, Alcala-Orozco CR, *et al*. Rapid Photocrosslinking of Silk Hydrogels with High Cell Density and Enhanced Shape Fidelity. *Adv Healthc Mater*. 2020;9(4):e1901667.

doi: 10.1002/adhm.201901667

23. Karimi F, Lau K, Kim HN, *et al*. Surface Biofunctionalization of Silk Biomaterials Using Dityrosine Cross-Linking. *ACS Appl Mater Interfaces*. 2022;14(28):31551-31566.

doi: 10.1021/acsami.2c03345

24. Roche CD, Gentile C. Transplantation of a 3D Bioprinted Patch in a Murine Model of Myocardial Infarction. *J Vis Exp*. 2020;(163).

doi: 10.3791/61675

25. O'Riordan CE, Trochet P, Steiner M, Fuchs D. Standardisation and future of preclinical echocardiography. *Mamm Genome*. 2023;34(2):123-155.

doi: 10.1007/s00335-023-09981-4

26. Mancuso A, Cianflone E, Cristiano MC, *et al*. Lyotropic Liquid Crystals: A Biocompatible and Safe Material for Local Cardiac Application. *Pharmaceutics*. 2022;14(2):452.

doi: 10.3390/pharmaceutics14020452

27. Feldman AT, Wolfe D. Tissue processing and hematoxylin and eosin staining. *Methods Mol Biol*. 2014;1180:31-43.

doi: 10.1007/978-1-4939-1050-2_3

28. Kim J, Choi W, Yoo D, *et al*. Solution-free and simplified H&E staining using a hydrogel-based stamping technology. *Front Bioeng Biotechnol*. 2023;11:1292785.

doi: 10.3389/fbioe.2023.1292785

29. Lattouf R, Younes R, Lutomski D, *et al*. Picrosirius red staining: a useful tool to appraise collagen networks in normal and pathological tissues. *J Histochem Cytochem*. 2014;62(10):751-758.

doi: 10.1369/0022155414545787

30. Li WJ, Yan H, Zhou ZY, *et al*. Cryptotanshinone Attenuated Pathological Cardiac Remodeling *In Vivo* and *In Vitro* Experiments. *Oxid Med Cell Longev*. 2023;2023:4015199.

doi: 10.1155/2023/4015199

31. Sridharan D, Pracha N, Dougherty JA, Akhtar A, Alvi SB, Khan M. A One-Stop Protocol to Assess Myocardial Fibrosis in Frozen and Paraffin Sections. *Methods Protoc*. 2022;5(1):13.

doi: 10.3390/mps5010013

32. Van De Vlekkert D, Machado E, d'Azzo A. Analysis of Generalized Fibrosis in Mouse Tissue Sections with Masson's Trichrome Staining. *Bio Protoc*. 2020;10(10):e3629.

doi: 10.21769/BioProtoc.3629

33. Dobin A, Davis CA, Schlesinger F, *et al*. STAR: ultrafast universal RNA-seq aligner. *Bioinformatics*. 2013;29(1):15-21.

doi: 10.1093/bioinformatics/bts635

34. Liao Y, Smyth GK, Shi W. featureCounts: an efficient general purpose program for assigning sequence reads to genomic features. *Bioinformatics*. 2014;30(7):923-930.

doi: 10.1093/bioinformatics/btt656

35. Love MI, Huber W, Anders S. Moderated estimation of

fold change and dispersion for RNA-seq data with DESeq2. *Genome Biol*. 2014;15(12):550.

doi: 10.1186/s13059-014-0550-8

36. R Core Team. R: A Language and Environment for Statistical Computing. R Foundation for Statistical Computing. Accessed June 9, 2023. http://www.R-project.org/

37. Corchete LA, Rojas EA, Alonso-López D, De Las Rivas J, Gutiérrez NC, Burguillo FJ. Systematic comparison and assessment of RNA-seq procedures for gene expression quantitative analysis. *Sci Rep*. 2020;10(1):19737.

doi: 10.1038/s41598-020-76881-x

38. Deshpande D, Chhugani K, Chang Y, *et al*. RNA-seq data science: From raw data to effective interpretation. *Front Genet*. 2023;14:997383.

doi: 10.3389/fgene.2023.997383

39. Koch CM, Chiu SF, Akbarpour M, *et al*. A Beginner's Guide to Analysis of RNA Sequencing Data. *Am J Respir Cell Mol Biol*. 2018;59(2):145-157.

doi: 10.1165/rcmb.2017-0430TR

40. Arif M, Klevstig M, Benfeitas R, *et al*. Integrative transcriptomic analysis of tissue-specific metabolic crosstalk after myocardial infarction. *eLife*. 2021;10:e66921.

doi: 10.7554/eLife.66921

41. Gehlenborg N, Wong B. Points of View: Heat maps. *Nat Methods*. 2012;9(3):213.

doi: 10.1038/nmeth.1902

42. Li X, Li B, Jiang H. Identification of timeseries differentially expressed genes and pathways associated with heart failure postmyocardial infarction using integrated bioinformatics analysis. *Mol Med Rep*. 2019;19(6):5281-5290.

doi: 10.3892/mmr.2019.10190

43. Zhang Q, Guo Y, Zhang B, *et al*. Identification of hub biomarkers of myocardial infarction by single-cell sequencing, bioinformatics, and machine learning. *Front Cardiovasc Med*. 2022;9:939972.

doi: 10.3389/fcvm.2022.939972

44. Majid QA, Fricker ATR, Gregory DA, *et al*. Natural Biomaterials for Cardiac Tissue Engineering: A Highly Biocompatible Solution. *Front Cardiovasc Med*. 2020;7:554597.

doi: 10.3389/fcvm.2020.554597

45. Settembrini A, Buongiovanni G, Settembrini P, *et al*. In-vivo evaluation of silk fibroin small-diameter vascular grafts: state of art of preclinical studies and animal models. *Front Surg*. 2023;10:1090565.

doi: 10.3389/fsurg.2023.1090565

46. Schneider KH, Goldberg BJ, Hasturk O, *et al*. Silk fibroin, gelatin, and human placenta extracellular matrix-based composite hydrogels for 3D bioprinting and soft tissue engineering. *Biomater Res*. 2023;27(1):117.

doi: 10.1186/s40824-023-00431-5

47. Johnston ER, Miyagi Y, Chuah JA, Numata K, Serban MA. The interplay between silk fibroin's structure and its adhesive properties. *ACS Biomater Sci Eng*. 2018;4(8):2815-2824.

doi: 10.1021/acsbiomaterials.8b00544

48. Lyu Y, Liu Y, He H, Wang H. Application of Silk-Fibroin-Based Hydrogels in Tissue Engineering. *Gels*. 2023;9(5):431.

doi: 10.3390/gels9050431

49. Pan X, Li R, Li W, *et al*. Silk fibroin hydrogel adhesive enables sealed-tight reconstruction of meniscus tears. *Nat Commun*. 2024;15(1):2651.

doi: 10.1038/s41467-024-47029-6

50. Patra C, Talukdar S, Novoyatleva T, *et al*. Silk protein fibroin from Antheraea mylitta for cardiac tissue engineering. *Biomaterials*. 2012;33(9):2673-2680.

doi: 10.1016/j.biomaterials.2011.12.036

51. Bazgir F, Nau J, Nakhaei-Rad S, *et al*. The Microenvironment of the Pathogenesis of Cardiac Hypertrophy. *Cells*. 2023;12(13):1780.

doi: 10.3390/cells12131780

52. Feng Y, Zhao G, Xu M, *et al*. rGO/Silk Fibroin-Modified Nanofibrous Patches Prevent Ventricular Remodeling *via* Yap/Taz-TGFβ1/Smads Signaling After Myocardial Infarction in Rats. *Front Cardiovasc Med*. 2021;8:718055.

doi: 10.3389/fcvm.2021.718055

53. Leite FG, Marana JF, de Sá LFT, *et al*. Effects of a collagen hyaluronic acid silk-fibroin patch with the electroconductive element polyaniline on left ventricular remodeling in an infarct heart model. *J Biomed Mater Res B Appl Biomater*. 2022;110(7):1651-1666.

doi: 10.1002/jbm.b.35026

54. Kopp A, Schunck L, Gosau M, *et al*. Influence of the Casting Concentration on the Mechanical and Optical Properties of FA/$CaCl_2$-Derived Silk Fibroin Membranes. *Int J Mol Sci*. 2020;21(18):6704.

doi: 10.3390/ijms21186704

55. Cai Y, Fu Y, Liu C, *et al*. Stathmin 1 is a biomarker for diagnosis of microvascular invasion to predict prognosis of early hepatocellular carcinoma. *Cell Death Dis*. 2022;13(2):176.

doi: 10.1038/s41419-022-04625-y

56. Kim MY, Seo EJ, Lee DH, *et al*. Gadd45beta is a novel mediator of cardiomyocyte apoptosis induced by ischaemia/hypoxia. *Cardiovasc Res*. 2010;87(1):119-126.

doi: 10.1093/cvr/cvq048

57. Kim YA, Kim MY, Yu HY, *et al*. Gadd45β is transcriptionally activated by p53 via p38α-mediated phosphorylation during myocardial ischemic injury. *J Mol Med*. 2013;91(11):1303-1313.

doi: 10.1007/s00109-013-1070-9

58. Wang J, Zhang G, Sui Y, *et al*. CD52 Is a Prognostic Biomarker and Associated With Tumor Microenvironment in Breast Cancer. *Front Genet*. 2020;11:578002.

doi: 10.3389/fgene.2020.578002

59. Zhang YF, Meng LB, Hao ML, Li XY, Zou T. CXCR4 and TYROBP mediate the development of atrial fibrillation via inflammation. *J Cell Mol Med*. 2022;26(12):3557-3567.

doi: 10.1111/jcmm.17405

60. Hedberg-Oldfors C, Abramsson A, Osborn DPS, *et al*. Cardiomyopathy with lethal arrhythmias associated with inactivation of KLHL24. *Hum Mol Genet*. 2019;28(11):1919-1929.

doi: 10.1093/hmg/ddz032

61. Shiba M, Higo S, Kondo T, *et al*. Phenotypic recapitulation and correction of desmoglein-2-deficient cardiomyopathy using human-induced pluripotent stem cell-derived cardiomyocytes. *Hum Mol Genet*. 2021;30(15):1384-1397.

doi: 10.1093/hmg/ddab127

62. Varillas-Delgado D. Role of the *PPARGC1A* Gene and Its rs8192678 Polymorphism on Sport Performance, Aerobic Capacity, Muscle Adaptation and Metabolic Diseases: A Narrative Review. *Genes*. 2024;15(12):1631.

doi: 10.3390/genes15121631

63. Yang D, Liu HQ, Yang Z, Fan D, Tang QZ. BMI1 in the heart: Novel functions beyond tumorigenesis. *EBioMedicine*. 2021;63:103193.

doi: 10.1016/j.ebiom.2020.103193

64. Baci D, Bosi A, Parisi L, *et al*. Innate Immunity Effector Cells as Inflammatory Drivers of Cardiac Fibrosis. *Int J Mol Sci*. 2020;21(19):7165.

doi: 10.3390/ijms21197165

65. Bahrami H, Sichetti F, Puppo E, *et al*. Physically-based simulation of elastic-plastic fusion of 3D bioprinted spheroids. *Biofabrication*. 2023;15(4):045021.

doi: 10.1088/1758-5090/acf2cb